Geometric origin of the intrinsic transverse spin transport in a canted-antiferromagnet/heavy-metal heterostructure

Wesley Roberts [1], Bowen Ma,[2] Martin Rodriguez-Vega [3,1] and Gregory A. Fiete [1,4]

[1]*Department of Physics, Northeastern University, Boston, Massachusetts 02115, USA*

[2]*Department of Physics and HK Institute of Quantum Science & Technology, The University of Hong Kong, Hong Kong, China*

[3]*Department of Physics, The University of Texas at Austin, Austin, Texas 78712, USA*

[4]*Department of Physics, Massachusetts Institute of Technology, Cambridge, Massachusetts 02139, USA*

(Received 17 January 2024; revised 28 April 2024; accepted 9 May 2024; published 21 May 2024)

We theoretically study the conditions under which an intrinsic spin Nernst effect–a transverse spin current induced by an applied temperature gradient–can occur in a canted-antiferromagnet insulator, such as $LaFeO_3$ and other materials of the same family. The spin Nernst effect may provide a microscopic mechanism for an experimentally observed anomalous thermovoltage in $LaFeO_3$/Pt heterostructures, where spin is transferred across the insulator/metal interface when a temperature gradient is applied to $LaFeO_3$ parallel to the interface [W. Lin *et al.*, Nat. Phys. **18**, 800 (2022)]. We find that $LaFeO_3$ exhibits an intrinsic spin Nernst effect when inversion symmetry is broken on the axes parallel to both the applied temperature gradient and the direction of spin transport, which can result in a spin injection across the insulator/metal interface. Our paper provides a general derivation of a symmetry-breaking-induced spin Nernst effect, which may open a path to engineering a finite spin Nernst effect in systems where it would otherwise not arise.

DOI: 10.1103/PhysRevB.109.174436

I. INTRODUCTION

The study of spin transport phenomena is vital to the growing field of spintronics [1,2], which seeks to use the spin degree of freedom to transfer energy or information, analogous to the use of electron charge in electronics. In particular, spin caloritronics considers thermally driven spin and heat flow in magnetic systems [3–5]. One area of growing interest in this field is magnonics [6–8], in which the relevant spin transport is mediated by magnons [9,10]—low-energy magnetic fluctuations that manifest as excitations above a magnetically ordered ground state. Magnons can exhibit topological transport effects such as a topological thermal Hall effect [11–20], where spin currents are driven by thermal gradients and deflected by Berry curvature effects [21]. However, due to the bosonic statistics of magnons, the thermal responses of magnons are not quantized (due to the absence of filled bands) as they are in the electronic analog where the Fermi statistics allow for a notion of a filled band. The study of magnon systems also has important technological potential originating in the transport of magnons as well as cavity magnonics [22].

In this paper, we theoretically explore spin transport in the antiferromagnetic insulator $LaFeO_3$ (LFO) [23–25], whose crystal structure and magnetic order are shown in Fig. 2. LFO has a perovskite structure [26] with space group *Pbnm*. Below its transition temperature, it has noncollinear antiferromagnetic order, with small spin canting giving rise to weak ferromagnetism along the *c* axis [27]. This weak ferromagnetism arises due to spin-oribit coupling effects that underlie anisotropy terms in the magnetic Hamiltonian [28,29]. In our paper, we explore a microscopic mechanism that could explain an experimentally observed anomalous thermovoltage in LFO/Pt heterostructures [30], where spin is transferred across the insulator/metal interface when a temperature gradient is applied to LFO *parallel* (and also perpendicular) to the interface. This spin transport is consistent with a spin Nernst effect (SNE) [31–38] in bulk LFO—however, under normal conditions, LFO does not support a SNE. We show that under sufficient lowering of the symmetries of LFO, namely, a loss of inversion symmetry along the directions of both the applied temperature gradient and the normal to the interface, a nonzero SNE arises. We argue that one way in which this lowered symmetry could manifest is through a weak magnetic dimerization along each of these axes. Although our paper is motivated by $LaFeO_3$, our analysis is more general and applicable to a broader class of antiferromagnetic materials with small canting.

We begin our discussion in Sec. II by briefly summarizing the observed transport phenomenon for which we propose a model. In Sec. III, we elaborate on the minimal model for LFO: We present its low-energy excitations in the form of magnons using a Holstein-Primakoff expansion. The magnon dispersion, Berry curvature, and spin Berry curvature are presented. We focus on aspects of the model that enforce a zero SNE. Next, in Sec. IV, we explore what constraints must be relaxed to achieve a nonzero SNE. The relevant symmetries prohibiting a finite SNE manifest most obviously in the spin Berry curvature. We present a Hamiltonian term that breaks these symmetries, and in Appendix C we show that this is the most general form of such a term. We then analyze the new magnon band structure and spin Berry curvature for the symmetry-broken model and present the temperature dependence of the (nonzero) SNE. Finally, in Sec. V, we conclude our discussion and provide an outlook for further work.

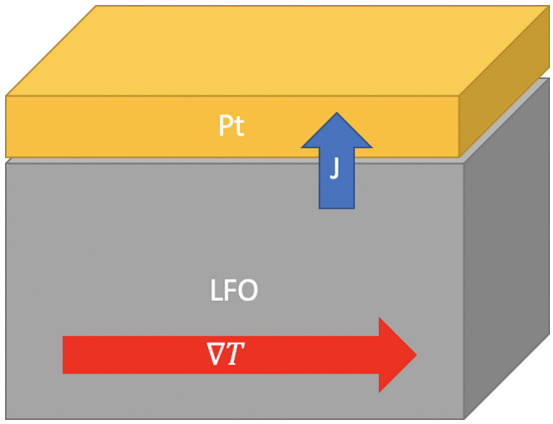

FIG. 1. Schematic of the experimental setup of Lin *et al.* [30], for which we discuss a microscopic mechanism. Pt is a heavy metal capping layer for $LaFeO_3$ (LFO). The red arrow indicates the direction of the temperature gradient ∇T and the blue arrow indicates the direction of the spin current J.

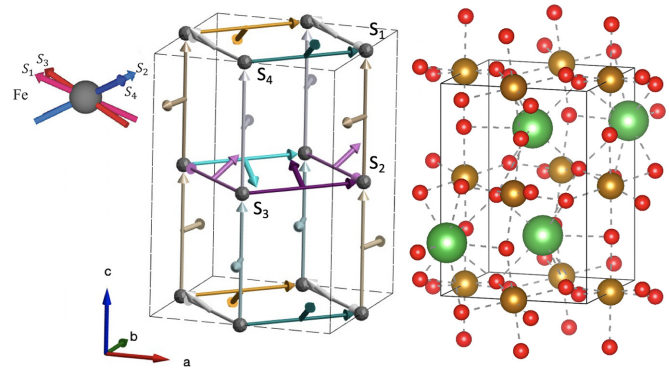

FIG. 2. Left: Ground-state configuration of LFO without an applied field, with DM coupling vectors depicted as arrows along the bonds between the spins. The c axis is ferromagnetic (has a small net moment), while the a and b axes are antiferromagnetic (have nearly canceling moments). Right: LFO unit cell, with oxygen atoms in red, iron in brown, and lanthanum in green.

II. EXPERIMENTAL TRANSPORT PHENOMENON

We begin with a brief discussion of the experimental setup that motivates our theoretical study [30]. In the experiment, a conductor with large spin-orbit coupling (Pt or W) was placed on a sample of LFO, an antiferromagnetic insulator, to which was applied a temperature gradient parallel to the interface (as well as perpendicular, but the more standard perpendicular orientation is not our focus here). Various directions and strengths of magnetic field were also applied, but the primary result, regardless of the magnetic field configuration, was a magnetothermovoltage observed in the conductor, ultimately due to spin pumping across the interface, which was detected as a voltage via the inverse spin Hall effect (hence the need for large atomic number metallic elements) [39–41].

The geometry of the device is depicted in Fig. 1. Note that a transverse spin current across the interface is not experimentally observed when LFO is replaced with a ferromagnetic insulator, unless a component of the temperature gradient is directed perpendicular to the interface to induce a longitudinal spin Seebeck effect [42].

We propose the spin Nernst effect (SNE) [33] as a candidate microscopic explanation for spin transport across the interface in the parallel temperature gradient geometry shown in Fig. 1. In the SNE, a transverse spin current with a given polarization is induced in the presence of a temperature gradient, so $J^{\mu}_{\nu} = \alpha^{\mu}_{\nu\beta}\nabla_{\beta}T$, where all the Greek indices take the values x, y, or z. The SNE amounts to cases in which $\alpha^{\mu}_{\nu\beta} \neq 0$ for $\nu \neq \beta$. However, as we discuss in the next section, bulk LFO does not on its own produce a nonzero SNE. Instead, it does so when its symmetry is sufficiently lowered—namely, when inversion symmetry is broken along the ν and β directions. This is detailed in Sec. IV.

III. PROPERTIES OF BULK $LaFeO_3$

$LaFeO_3$ (Fig. 2) is a member of the rare-earth orthoferrites [23,24,43–46]. The Fe atoms have spin 5/2, inviting an analysis of spin fluctuations in the language of magnon quasiparticles. The transition temperature of LFO is 738 K [23], and is therefore a magnetically ordered insulator at room temperature. We take as a starting point a Hamiltonian with nearest-neighbor Dzyaloshinsky-Moriya interactions (DMI) [28,29] mediated by the oxygen atoms lying between neighboring Fe atoms. Contrary to the structure of other perovskites, the Pbnm structure of LFO supports a nonvanishing DMI, where only canted G-type AFM order is allowed [30]. The existence of a DMI in LFO is responsible for the small canting in the magnetic order, which ultimately allows for nontrivial Berry curvature and spin Berry curvature in the magnon bands, discussed in detail below.

The minimal magnetic Hamiltonian for LFO is given by [23]

$$\begin{aligned} H = {} & J_c \sum_{\text{along } c} \vec{S}^L_i \cdot \vec{S}^L_j + J_{ab} \sum_{ab \text{ plane}} \vec{S}^L_i \cdot \vec{S}^L_j \\ & + J' \sum_{\langle\langle i,j\rangle\rangle} \vec{S}^L_i \cdot \vec{S}^L_j + \sum_{\langle i,j\rangle} \vec{D}_{ij} \cdot \vec{S}^L_i \times \vec{S}^L_j \\ & + K_a \sum_i \left(S^{Lx}_i\right)^2 + K_c \sum_i \left(S^{Lz}_i\right)^2 + \sum_i \vec{h} \cdot \vec{S}^L_i, \end{aligned} \quad (1)$$

where the L superscript indicates that the spins are written in a global lab frame, with the a, b, and c axes corresponding to the x, y, and z directions, respectively. The Fe atoms have a $S = 5/2$ moment. Here J_c is the nearest-neighbor magnetic exchange energy along the c axis, J_{ab} the nearest-neighbor magnetic exchange in the ab plane, J' the second-nearest-neighbor exchange, $\vec{D}_{ij}$ the Dyzaloshinskii-Moriya interaction between site i and j, K_a the Ising anistropy in the ab plane along the x direction, K_c the Ising anistropy along the c axis in the z direction, and $\vec{h}$ is an externally applied magnetic field present in the experiments, where field directions were chosen both along the plane of the interface and perpendicular to the interface [30]. Thus, in what follows we present results for an applied field with both of these components nonzero. The parameters in Eq. (1) have been found via inelastic neutron scattering [23] and are collected in Table I.

TABLE I. List of LFO parameters appearing in Eq. (1). Magnitudes for DMI are given as D_{ab} and D_c for the nearest-neighbor DM couplings in the ab plane and along the c axis, respectively. In what follows, we choose the applied magnetic field to be $h = (0, 1, 1)$, as described below.

LFO parameters (meV)			
J_c		5.47	
J_{ab}		5.47	
J'		0.24	
D_{ab}		0.130	
D_c		0.158	
K_a		−0.0124	
K_c		−0.0037	
	$\vec{D}_{ij} = D_{ij}(\alpha_{ij}, \beta_{ij}, \gamma_{ij})$		
	$\|\alpha\|$	$\|\beta\|$	$\|\gamma\|$
D_{ab}	0.554	0.553	0.623
D_c	0.191	0.982	0

We treat the low-energy bosonic degrees of freedom in LFO using a Holstein-Primakoff (HP) transformation [9,47–49] which represents the spins in terms of bosonic creation operators $a^\dagger$ and annihilation operators a,

$$S^z = S - a^\dagger a, \tag{2}$$

$$S^+ = \sqrt{2S}\sqrt{1 - \frac{a^\dagger a}{2S}}\, a \approx \sqrt{2S}a, \tag{3}$$

$$S^- = \sqrt{2S}a^\dagger\sqrt{1 - \frac{a^\dagger a}{2S}} \approx \sqrt{2S}a^\dagger, \tag{4}$$

where the approximation is the lowest-order term in a Taylor series in $1/S$. The HP bosons are defined relative to a local reference frame in which the z axis aligns with the z component of the spin at that position in the classical ground state. S^α and $S^{L\alpha}$ are therefore related by

$$\vec{S}_i^L = R_i \vec{S}_i, \tag{5}$$

where the rotation matrix R_i rotates a vector along the local z axis at position i into the direction of the ground-state spin at i.

To find the ground-state magnetic configuration, minimization of the classical energy (spins treated as classical variables) is performed via the assumption of a four-sublattice unit cell due to the small canting introduced by the DMI. Without an applied magnetic field, the classical texture is given by

$$\begin{aligned}
\vec{S}_1^L &= S(-\cos\theta\sin\phi, -\cos\theta\cos\phi, \sin\theta),\\
\vec{S}_2^L &= S(\cos\theta\sin\phi, \cos\theta\cos\phi, \sin\theta),\\
\vec{S}_3^L &= S(-\cos\theta\sin\phi, \cos\theta\cos\phi, \sin\theta),\\
\vec{S}_4^L &= S(\cos\theta\sin\phi, -\cos\theta\cos\phi, \sin\theta),
\end{aligned} \tag{6}$$

with $\theta = 0.52^\circ$ giving a small ferromagnetic canting along the c axis and $\phi = 0.46^\circ$ giving antiferromagnetic canting within the ab plane [23].

A. Dispersion and band Berry curvature

Expanding around the classical spin configuration above using a $1/S$ expansion, our Hamiltonian takes the form

$$H \approx \frac{1}{2}\sum_{\mathbf{r},\vec{\delta}} \psi^\dagger(\mathbf{r}) H_{\vec{\delta}} \psi(\mathbf{r} + \vec{\delta}), \tag{7}$$

where $\mathbf{r}$ labels the lattice site and $\vec{\delta}$ are the relevant nearest- and next-nearest-neighbor separation vectors. $\psi(\mathbf{r})$ is a Nambu spinor, given by

$$\psi(\mathbf{r}) = \begin{pmatrix} a_1(\mathbf{r}) \\ a_2(\mathbf{r}) \\ a_3(\mathbf{r}) \\ a_4(\mathbf{r}) \\ a_1^\dagger(\mathbf{r}) \\ a_2^\dagger(\mathbf{r}) \\ a_3^\dagger(\mathbf{r}) \\ a_4^\dagger(\mathbf{r}) \end{pmatrix}. \tag{8}$$

The noncollinearity of the classical spin configuration will introduce pairing of Holstein-Primakoff magnons (i.e., number non-conserving terms), and thus the Nambu representation is necessary. Here, we have eliminated linear bosonic terms by expanding around the energetic minimum, and we have dropped constants as well as interaction terms of three bosonic operators and higher, consistent with a Taylor expansion in $(1/S)$ of the HP transformation.

Performing a Fourier transform as detailed in Appendix A results in the form

$$H = \sum_{\mathbf{k}} \psi_{\mathbf{k}}^\dagger H_{\mathbf{k}} \psi_{\mathbf{k}}, \tag{9}$$

where the k-space Nambu spinors are given by

$$\psi_{\mathbf{k}} = \begin{pmatrix} a_1(\mathbf{k}) \\ a_2(\mathbf{k}) \\ a_3(\mathbf{k}) \\ a_4(\mathbf{k}) \\ a_1^\dagger(-\mathbf{k}) \\ a_2^\dagger(-\mathbf{k}) \\ a_3^\dagger(-\mathbf{k}) \\ a_4^\dagger(-\mathbf{k}) \end{pmatrix}.$$

Thus, solving the Fourier-transformed problem amounts to diagonalizing the matrix H_k. However, care must be taken to ensure that the transformation T_k such that $T_k^\dagger H_k T_k = \Lambda_k$ (with Λ_k diagonal) also preserves the bosonic commutation relations

$$[\psi_k, \psi_k^\dagger] = \begin{pmatrix} I_4 & 0 \\ 0 & -I_4 \end{pmatrix} \equiv \eta, \tag{10}$$

so in the diagonal problem $H = \sum_k \Lambda_k \gamma_k^\dagger \gamma_k$ the operators $\gamma_k^\dagger \gamma_k$ are number operators. It turns out that for this to be the case, T_k must be a paraunitary transformation [9,50–52],

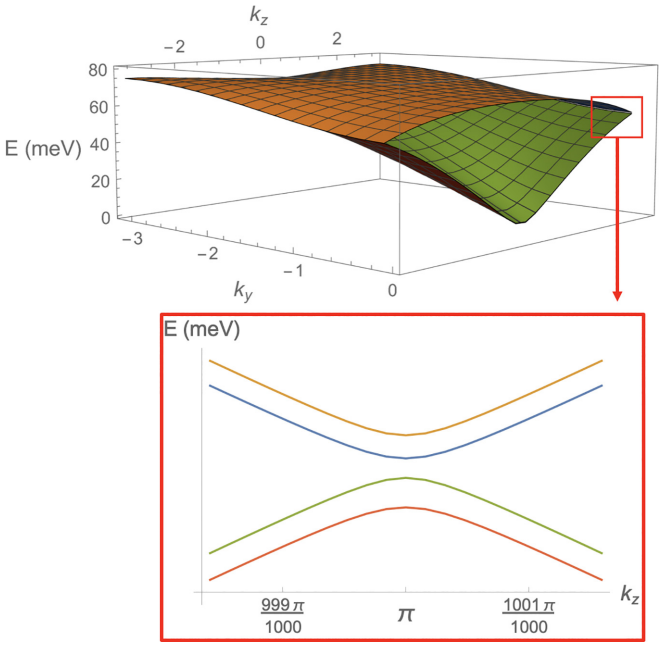

FIG. 3. Top: Magnon dispersion $E(0, k_y, k_z)$ for $LaFeO_3$ with an applied field $h = (0, 1, 1)$. All four particle bands are pictured, with two nearly degenerate upper and two nearly degenerate lower bands. Bottom: Magnon dispersion for $LaFeO_3$ with applied field $h = (0, 1, 1)$ near $(0, 0, \pi)$. A small gap is present, allowing for topological quantities to be computed for each band individually.

which means

$$T_k \eta T_k^\dagger = \eta. \tag{11}$$

Note that Eq. (11) implies that rather than diagonalize H_k via similarity transformation in the usual way, the eigenvalue problem we should solve to obtain the magnon dispersion is

$$\eta H_k \left|\psi_k^n\right\rangle = E_k^n \left|\psi_k^n\right\rangle. \tag{12}$$

The kets $|\psi_k^n\rangle$ that solve the eigenproblem are columns of T_k, and from paraunitarity they inherit the normalization condition:

$$\left\langle\psi_k^m\right|\eta\left|\psi_k^n\right\rangle = \eta_{mn}. \tag{13}$$

We call solutions with norm 1 particle bands and those with norm -1 hole bands. Equivalently, the bands with positive eigenenergies (norm 1) are physical particle bands and the bands with opposite signs are the hole partners. Using this formalism, it is possible to obtain the magnon band structure for LFO, plotted in Fig. 3. Bulk LFO features pairs of nearly degenerate bands, as well as near fourfold degeneracies along the Brillouin zone boundary; both of these features make important contributions to the behavior of the SNE.

In addition to the band structure, we can define magnon Berry curvature and Chern numbers. These are defined with respect to the eigenstates in Eq. (12). We first define a Berry connection for the band n as

$$A_\mu^n = -i\eta_{nn}\left\langle\psi_k^n\right|\eta\partial_\mu\left|\psi_k^n\right\rangle. \tag{14}$$

The Berry curvature is then naturally expressed as [53]

$$\Omega_{\mu\nu}^n = \partial_\mu A_\nu^n - \partial_\nu A_\mu^n. \tag{15}$$

Finally, the Berry curvature can be used to compute a Chern number by integrating over the first Brillouin zone:

$$C^n = \frac{1}{2\pi}\int d^2k\,\Omega_{xy}^n. \tag{16}$$

As evident from the formula, which involves a two-dimensional momentum space integral, the Chern number (as well as the spin Nernst response) is an inherently two-dimensional concept. Therefore, to discuss it meaningfully, we restrict ourselves to an appropriate two-dimensional problem. Ultimately, we will want to consider the flow of spin in the z direction, with an in-plane temperature gradient which we take to be directed along the y axis. This geometry naturally invites us to consider a yz plane when computing topological quantities. When computing the total Nernst response, we sum over two-dimensional contributions from all planes. That is, if $\alpha_{\nu\beta}^\mu(k_x)$ is the contribution to the SNE from the k_x plane, then the total response will be given by $\alpha_{\nu\beta}^\mu = \int dk_x\,\alpha_{\nu\beta}^\mu(k_x)$ [54].

Finally, we note that Ω^n can be represented in the Thouless-Kohmoto-Nightingale-Nijs (TKNN) [55] form derived from linear response theory, analogous to the one we will present for the spin Berry curvature,

$$\Omega_{\mu\nu}^n(k) = \sum_{m\neq n}\eta_{nn}\eta_{mm}\frac{2\mathrm{Im}\left\langle\psi_k^n\right|\partial_\mu H_k\left|\psi_k^m\right\rangle\left\langle\psi_k^n\right|\partial_\nu H_k\left|\psi_k^m\right\rangle}{(E_{nk}-E_{mk})^2}, \tag{17}$$

where the sum is taken over both particle and hole bands. The quantity $\Omega_{zy}^n(k_x = 0)$ for each particle band is plotted in Fig. 4. We see that each band is topologically trivial ($C^n = 0$) because when integrating over the BZ, each point of positive curvature is canceled by another of negative curvature; this is from the symmetries $\Omega_{zy}^n(k_x, k_y, k_z) = -\Omega_{zy}^n(-k_x, -k_y, k_z)$ and $\Omega_{zy}^n(k_x, k_y, k_z) = -\Omega_{zy}^n(k_x, k_y, -k_z)$, either of which alone is enough to enforce $C^n = 0$.

Next, we look at the SNE itself. The spin-current continuity equation is written as $\frac{\partial\vec{s}}{\partial t} = -\nabla\cdot\vec{j}_S + \vec{\tau}_S$ [11,31,56,57]. In an inversion-symmetric system, the torque term $\vec{\tau}_S$ does not contribute to the SNE. The response tensor α is given by [11,31]

$$J_\lambda^\gamma = \alpha_{\lambda\beta}^\gamma\nabla_\beta T = \frac{2k_B}{V}\sum_n\sum_k\Omega_{\lambda\beta}^{n\gamma}c_1[g(E_{nk})]\nabla_\beta T, \tag{18}$$

where $g(E)$ is the Bose occupation factor and $c_1(x) = (1+x)\ln(x) - x\ln(x)$. The sum $\sum_n$ is over only particle bands and the sum $\sum_k$ is taken over all three dimensions. Here γ is the polarization of the spin current, λ is the direction of the spin current, and β is the direction of the temperature gradient (each of which could be along x, y, or z). The quantity $\Omega_{\lambda\beta}^{n\gamma}$ is the spin Berry curvature, a generalization of the band Berry curvature $\Omega_{\mu\nu}^n$. Analogous to Eq. (17), it is given by [11,32],

$$\Omega_{\beta\gamma}^{n\alpha}(k) = \sum_{m\neq n}\eta_{nn}\eta_{mm}\frac{2\mathrm{Im}\left\langle\psi_k^n\right|j_\beta^\alpha\left|\psi_k^m\right\rangle\left\langle\psi_k^n\right|\partial_\gamma H_k\left|\psi_k^m\right\rangle}{(E_{nk}-E_{mk})^2}, \tag{19}$$

where j_β^α is the spin current operator in the Bogoliubov-de Gennes (BdG) representation (see Appendices A and B for pedagogical discussion of BdG formalism). The spin current operator is given by

$$j_\beta^\alpha = \tfrac{1}{4}(\partial_\beta H_k\eta\Sigma^\alpha + \Sigma^\alpha\eta\partial_\beta H_k), \tag{20}$$

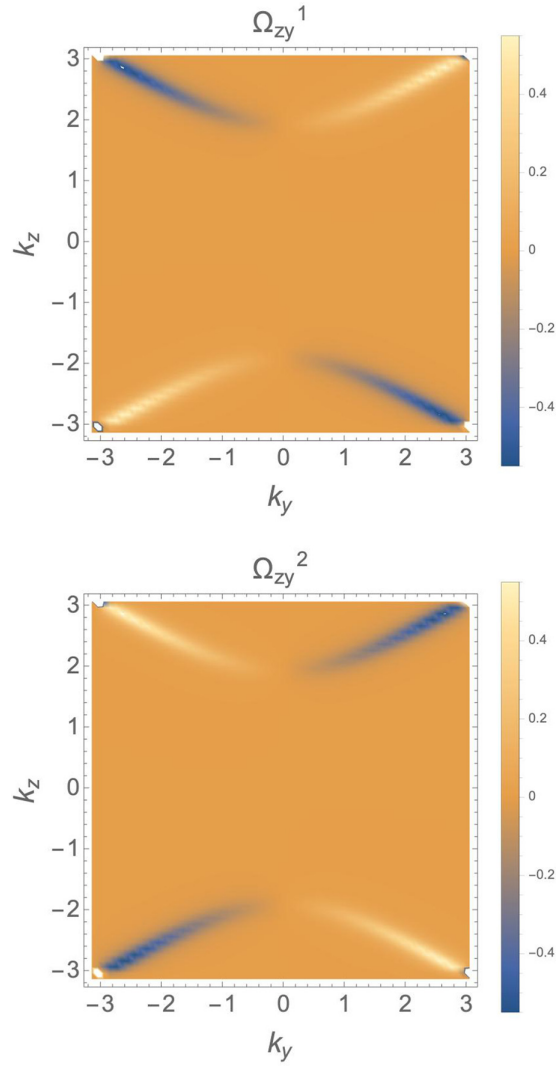

FIG. 4. Magnon Berry curvature $\Omega^n_{zy}(0, k_y, k_z)$ for $LaFeO_3$ with applied field $h = (0, 1, 1)$, for $n = 1, 2$. The lower bands $n = 3, 4$ have mostly trivial Berry curvature, with hot spots only at corners, shown in Appendix D.

with $\Sigma^\alpha = \mathrm{diag}(S^\alpha_1, S^\alpha_2, S^\alpha_3, S^\alpha_4, S^\alpha_1, S^\alpha_2, S^\alpha_3, S^\alpha_4)$ encoding the magnon polarization, for S^α_i the classical spin configuration. Figure 10 depicts the spin Berry curvature, $\Omega^{nx}_{zy}(0, k_y, k_z)$, for each band. We find the symmetries

$$\Omega^{nx}_{zy}(k_x, k_y, k_z) = -\Omega^{nx}_{zy}(-k_x, -k_y, k_z)$$

and

$$\Omega^{nx}_{zy}(k_x, k_y, k_z) = -\Omega^{nx}_{zy}(k_x, k_y, -k_z),$$

which taken together with the corresponding symmetries of the bands $E_n(k_i) = E_n(-k_i)$ (in other words, changing the sign of any k_i does not change the energy) lead to a vanishing SNE within each band. Whereas the symmetries of the dispersion did not matter in the cancellation of the Chern number, they are important here because they enter through the Bose occupation function g.

Now that we have discussed the relevant features of unperturbed bulk LFO, we turn next to an analysis of what sorts of modifications to the model would create a nonzero SNE. A weak dimerization will turn out to play an important role in producing a finite intrinsic SNE.

We note that while we study the intrinsic, Berry-curvature-based contribution to the SNE, there may also be an extrinsic contribution [31,58]. Because it arises due to magnon scattering, the extrinsic effect depends sensitively on the magnon lifetime. The magnon lifetime depends on both **k** and temperature, and a detailed calculation amounts to a study in its own right. Rather than undertaking such a calculation, we make two important notes before moving to a discussion of the intrinsic SNE. To do so, we compute the extrinsic response as in Eq. (S.25a) of Ref. [31], using the same parameters as for the intrinsic response. For a preliminary study, we computed the response using $k_BT = 50$ meV, which is comfortably below the Curie temperature.

First, we find that (assuming a constant magnon lifetime) the extrinsic effect does not arise in bulk LFO with symmetries intact. Second, the extrinsic effect does arise under the same symmetry-breaking terms we will discuss below. Based on our direct calculations of the extrinsic contribution, for short magnon lifetimes (assuming mean-free paths on the order of single unit cells as a lower limit) the extrinsic effect can be up to the same order of magnitude and of the same sign as the intrinsic effect. In the present paper, we focus on the symmetry-breaking-induced intrinsic SNE, but we note that there can be an additional extrinsic effect requiring detailed estimation of the magnon lifetime [59].

IV. SYMMETRY BREAKING AND SPIN NERNST EFFECT

We begin by asking a general question: At the level of the BdG Hamiltonian H_k, what symmetries would need to be lowered in order to produce a finite SNE? We have already begun to discuss this above when we commented on the elimination of both the Chern numbers and the SNE within each band as well as between bands—the intraband cancellation occurs due to k-space symmetries in the Berry curvature.

A. k-space symmetry

The intraband symmetry that leads to the vanishing of the SNE manifests at the level of the BdG Hamiltonian as

$$H(k_x, k_y, k_z) = H(k_x, k_y, -k_z), \tag{21}$$

$$H(k_x, k_y, k_z) = H(k_x, -k_y, k_z), \tag{22}$$

where for clarity we have switched to notation where $H_{\mathbf{k}} = H(k_x, k_y, k_z)$. We note at the outset that not only will breaking these symmetries create a net SNE via Eq. (18) but it can also create a source term contribution due to $H_{\mathbf{k}} \neq H_{-\mathbf{k}}$. Below we focus on the contribution from the current term rather than the source term. The presence of a source term due to inversion-symmetry breaking will lead to some dissipation; however, all of our results will apply within the window of the spin relaxation time [57].

We first consider the $k_z \to -k_z$ symmetry. For a term to break this symmetry, it must appear in the Hamiltonian in the form

$$[H_\Delta(k_z)]_{ij} = \Delta_{ij} \sin(k_z l_{ij}), \tag{23}$$

(or in some other odd function of k_z) where we are so far not restricting the elements of this term in particle-hole space but are simply enforcing that the whole term is odd in k_z. Since any term with the property $f(k) \neq f(-k)$ can be written in terms of its Fourier components, terms of the form Eq. (23) with various l_{ij} are sufficient to specify any inversion-breaking term. We can therefore simply ask what sort of term at the level of the spin Hamiltonian gives rise to a bosonic term of the form Eq. (23).

If we restrict ourselves only to nearest-neighbor couplings that break inversion symmetry, then it turns out that the most general form of the symmetry-breaking term is (see Appendix C)

$$H_\Delta = \frac{1}{4}\sum_j \Gamma^{\alpha\beta}\left(S^\alpha_{aj}S^\beta_{bj-1} - S^\alpha_{aj}S^\beta_{bj}\right), \tag{24}$$

where we do not enforce a specific form for $\Gamma^{\alpha\beta}$, except that it be real, which is required for H_Δ to be Hermitian. The sum on j is taken along the axis on which the symmetry is to be broken. Rotating into the local frame such that $\tilde{\Gamma}^{\alpha\beta} = \Gamma^{\gamma\delta}R^{\gamma\alpha}_a R^{\delta\beta}_b$ and performing the Holstein-Primakov transformation and Fourier transformations, we find that

$$\begin{aligned} H^{x,y}_\Delta = \frac{1}{4}\sum_d\sum_k (-1)^d[&(\tilde{\Gamma}^{xx} - \tilde{\Gamma}^{yy} - i\tilde{\Gamma}^{xy} - i\tilde{\Gamma}^{yx})e^{-ik(d+x_b)}a_k b_{-k} + (\tilde{\Gamma}^{xx} + \tilde{\Gamma}^{yy} + i\tilde{\Gamma}^{xy} - i\tilde{\Gamma}^{yx})e^{-ik(d+x_b)}a_k b^\dagger_k \\ &- (\tilde{\Gamma}^{xx} + \tilde{\Gamma}^{yy} - i\tilde{\Gamma}^{xy} + i\tilde{\Gamma}^{yx})e^{ik(d+x_b)}a^\dagger_k b_k - (\tilde{\Gamma}^{xx} - \tilde{\Gamma}^{yy} + i\tilde{\Gamma}^{xy} + i\tilde{\Gamma}^{yx})e^{ik(d+x_b)}a^\dagger_k b^\dagger_{-k}], \end{aligned}$$

where $H^{x,y}_\Delta$ denotes that we are only considering the (x, y) elements of $\tilde{\Gamma}$. Here $\sum_d$ is over the nearest-neighbor displacements $d = 0, -1$ and $x_b = 1/2$ is the separation between a and b sublattices. We see that when we carry out the d sum, the factor $(-1)^d$ is what creates odd k dependence. This factor comes, in particular, from the relative minus sign between coupling of S^α_{aj} to S^β_{bj} and S^β_{bj-1}. Performing this sum, we explicitly find

$$\begin{aligned} H^{x,y}_\Delta = \frac{-i}{2}\sum_k \sin(k/2)[&(\tilde{\Gamma}^{xx} - \tilde{\Gamma}^{yy} - i\tilde{\Gamma}^{xy} - i\tilde{\Gamma}^{yx})a_k b_{-k} \\ &+ (\tilde{\Gamma}^{xx} + \tilde{\Gamma}^{yy} + i\tilde{\Gamma}^{xy} - i\tilde{\Gamma}^{yx})a_k b^\dagger_k \\ &- (\tilde{\Gamma}^{xx} + \tilde{\Gamma}^{yy} - i\tilde{\Gamma}^{xy} + i\tilde{\Gamma}^{yx})a^\dagger_k b_k \\ &- (\tilde{\Gamma}^{xx} - \tilde{\Gamma}^{yy} + i\tilde{\Gamma}^{xy} + i\tilde{\Gamma}^{yx})a^\dagger_k b^\dagger_{-k}]. \end{aligned}$$

Note that in the presence of an inversion-breaking term, the BdG Hamiltonian is not sensitive to the particular form of Γ but rather depends on the presence of opposite coupling between forward and backward nearest neighbors.

We have so far found a general form for spin coupling along some direction which introduces k-space inversion-breaking terms along that direction in the BdG Hamiltonian. It is useful to note a special feature of this term, which happens to make its analysis simpler. In principle, when one adds H_Δ to the original Hamiltonian, one should minimize the classical energy once again to find the new classical ground state. However, for the form we have proposed, if one restrict themselves to the four-sublattice problem as we have for unperturbed LFO, H_Δ turns out not to modify the classical energy, and therefore does not modify the canting. This is because in the classical limit H_Δ becomes, for a uniform spin configuration,

$$H_\Delta = \frac{1}{4}\sum_j \tilde{\Gamma}^{\alpha\beta}\left(S^\alpha_a S^\beta_b - S^\alpha_a S^\beta_b\right) = 0, \tag{25}$$

for any arrangement where each sublattice is uniform from site to site—for example, where there is not a spiral texture along a sublattice.

To check that it is sensible to proceed with this uniform-sublattice assumption, one can check that H_Δ does not introduce linear boson operators when one performs the HP expansion: If it were to introduce linear terms, this would indicate that one were not expanding around an energy minimum anymore. To see that linear terms are not introduced for any choice of rotations, we let $i = x, y$ and write out the only terms that are able to contribute linear terms, which are those involving $S^i_j S^z_l$. The terms in H_Δ that could generate linear a bosons are

$$\sum_j \tilde{\Gamma}^{iz}\left(S^i_{aj}S^z_{bj-1} - S^i_{aj}S^z_{bj}\right) = \sum_j \tilde{\Gamma}^{iz}S^i_{aj}\left(S^z_{bj-1} - S^z_{bj}\right). \tag{26}$$

When one performs the HP transformation on S^z, the $\mathcal{O}(S)$ terms that would normally contribute a linear term cancel one another:

$$\begin{aligned} &\textstyle\sum_j \tilde{\Gamma}^{iz}S^i_{aj}(S - b^\dagger_{j-1}b_{j-1} - S + b^\dagger_j b_j) \\ &\quad = \textstyle\sum_j \tilde{\Gamma}^{iz}S^i_{aj}(-b^\dagger_{j-1}b_{j-1} + b^\dagger_j b_j). \end{aligned} \tag{27}$$

The only contributions from these kinds of terms are boson interactions, which we drop in the $1/S$ expansion. A similar argument holds if we look for the corresponding terms that would generate linear b bosonic terms. Therefore, we find that

(1) H_Δ does not modify the classical ground state configuration.

(2) The lowest-order bosonic terms H_Δ contributing to the Hamiltonian are quadratic.

Therefore, we can safely proceed with adding terms of the form H_Δ to the Hamiltonian, without needing to find a new energetic minimum configuration. In fact, no z-spin components contribute nonzero boson terms except at higher than quadratic order. Therefore, the expression we wrote for $H^{x,y}_\Delta$ is already the full expression for H_Δ to quadratic order. Expressing it in BdG-doubled form, we have

$$H_\Delta^c = \frac{-i}{4}\sum_k \sin(k/2)[(\tilde{\Gamma}^{xx} - \tilde{\Gamma}^{yy} - i\tilde{\Gamma}^{xy} - i\tilde{\Gamma}^{yx})(b_{-k}a_k - a_{-k}b_k) + (\tilde{\Gamma}^{xx} + \tilde{\Gamma}^{yy} + i\tilde{\Gamma}^{xy} - i\tilde{\Gamma}^{yx})(b_k^\dagger a_k - a_{-k}b_{-k}^\dagger)$$
$$- (\tilde{\Gamma}^{xx} + \tilde{\Gamma}^{yy} - i\tilde{\Gamma}^{xy} + i\tilde{\Gamma}^{yx})(a_k^\dagger b_k - b_{-k}a_{-k}^\dagger) - (\tilde{\Gamma}^{xx} - \tilde{\Gamma}^{yy} + i\tilde{\Gamma}^{xy} + i\tilde{\Gamma}^{yx})(a_k^\dagger b_{-k}^\dagger - b_k^\dagger a_{-k}^\dagger)]. \quad (28)$$

The c superscript denotes that this is valid for couplings along the c axis, because so far we have assumed that the coupled spins are arranged along a line parallel to the axis along which the inversion symmetry is being broken. This is true of couplings between S_1 and S_2 as well as between S_3 and S_4, which lie along the c axis and break k_z inversion. However, couplings along the b axis which break the k_y symmetry are slightly more complicated due to the fact that nearest neighbors are not separated by just $\hat{y}/2$ but instead by $\frac{\pm\hat{x}+\hat{y}}{2}$. The result is that couplings in the ab plane take the form

$$H_\Delta^{ab} = \frac{-i}{2}\sum_k \cos(k_x/2)\sin(k_y/2)[(\tilde{\Gamma}^{xx} - \tilde{\Gamma}^{yy} - i\tilde{\Gamma}^{xy} - i\tilde{\Gamma}^{yx})(b_{-k}a_k - a_{-k}b_k) + (\tilde{\Gamma}^{xx} + \tilde{\Gamma}^{yy} + i\tilde{\Gamma}^{xy} - i\tilde{\Gamma}^{yx})(b_k^\dagger a_k - a_{-k}b_{-k}^\dagger)$$
$$- (\tilde{\Gamma}^{xx} + \tilde{\Gamma}^{yy} - i\tilde{\Gamma}^{xy} + i\tilde{\Gamma}^{yx})(a_k^\dagger b_k - b_{-k}a_{-k}^\dagger) - (\tilde{\Gamma}^{xx} - \tilde{\Gamma}^{yy} + i\tilde{\Gamma}^{xy} + i\tilde{\Gamma}^{yx})(a_k^\dagger b_{-k}^\dagger - b_k^\dagger a_{-k}^\dagger)]. \quad (29)$$

Including the terms in Eqs. (28) and (29), the Hamiltonian has the effect of creating a nonzero contribution to the SNE from each individual band. However, for large enough perturbations, there is not only a net contribution from each band, but a total contribution when summed over bands, resulting in a finite SNE. This is shown explicitly below.

B. Physical model for symmetry breaking

For concreteness, we consider a model with exchangelike symmetry-breaking coupling of the form

$$H_\Delta = \sum_j \Delta\left(S_{aj}^\alpha S_{bj-1}^\alpha - S_{aj}^\alpha S_{bj}^\alpha\right). \quad (30)$$

We begin by noting that a possible origin of a term like this can be considered by absorbing H_Δ into the relevant exchange term of a magnetic Hamiltonian, $H_J = J\sum_j (S_{aj}^\alpha S_{bj}^\alpha + S_{aj}^\alpha S_{bj-1}^\alpha)$. Collecting terms, we see that

$$H_J + H_\Delta = \sum_j \left((J+\Delta)S_{aj}^\alpha S_{bj-1}^\alpha + (J-\Delta)S_{aj}^\alpha S_{bj}^\alpha\right). \quad (31)$$

Thus, the effect of the symmetry-breaking term H_Δ is to create a difference Δ between the exchange coupling for atoms within the same unit cell and those in different unit cells. This would occur, for example, in the case of dimerization along the axis of symmetry breaking.

In LFO, we require symmetry breaking along the y and z axes. We therefore require the full inversion-breaking term to be

$$\begin{aligned} H_\Delta = \sum_r \big[&\Delta\left(S_1^\alpha(\vec{r})S_2^\alpha(\vec{r}-\hat{e}_c) - S_1^\alpha(\vec{r})S_2^\alpha(\vec{r})\right) \\ &+ \Delta\left(S_4^\alpha(\vec{r})S_3^\alpha(\vec{r}-\hat{e}_c) - S_4^\alpha(\vec{r})S_3^\alpha(\vec{r})\right) \\ &+ \Delta\left(S_1^\alpha(\vec{r})S_4^\alpha(\vec{r}-\hat{e}_b) - S_1^\alpha(\vec{r})S_4^\alpha(\vec{r})\right) \\ &+ \Delta\left(S_1^\alpha(\vec{r})S_4^\alpha(\vec{r}-\hat{e}_b-\hat{e}_a) - S_1^\alpha(\vec{r})S_4^\alpha(\vec{r}-\hat{e}_a)\right) \\ &+ \Delta\left(S_2^\alpha(\vec{r})S_3^\alpha(\vec{r}-\hat{e}_b) - S_2^\alpha(\vec{r})S_3^\alpha(\vec{r})\right) \\ &+ \Delta\left(S_2^\alpha(\vec{r})S_3^\alpha(\vec{r}-\hat{e}_b-\hat{e}_a) - S_2^\alpha(\vec{r})S_3^\alpha(\vec{r}-\hat{e}_a)\right)\big]. \end{aligned} \quad (32)$$

Couplings along the c axis produce magnon terms of the form H_Δ^c [Eq. (28)], while couplings in the ab plane (which break the k_y inversion symmetry) produce terms of the form H_Δ^{ab} [Eq. (29)]. We can now ask about what changes occur to the band structure, Berry curvature, and SNE when Eq. (32) is added to the Hamiltonian.

For small perturbation strengths, we recover a nonzero bandwise SNE; however, while the contributions from individual bands are nonzero, as is expected because of the lower symmetry of Ω_{zy}^x, the effects from nearly degenerate bands cancel one another, leading to a vanishing total SNE. For example, at $\Delta = 0.01$ meV and $k_BT = 100$ meV, we find that for the highest band $|\alpha_{zy}^{1x}|/k_BT = 0.033$, where $\alpha_{zy}^x = \sum_n \alpha_{zy}^{nx}$ with the sum taken over particle bands, but $\alpha_{zy}^x = 0$.

However, when we increase the perturbation size we find that large spin Berry curvature hot spots are created (see Fig. 5), which are large enough to overcome the effect of near-degenerate bands with opposite Ω_{zy}^{nx}. When Ω_{zy}^{nx} is small, the fact that the two highest and two lowest bands are nearly degenerate leads to cancellation of the SNE in Eq. (18); when Ω_{zy}^{nx} becomes large in some region, even a small gap leading to a small difference in the Bose occupation factor is enough to obtain a net effect. For example, we find that for $\Delta/J = 0.1$ the SNE increases to $\alpha_{zy}^x/k_BT = 2.5\times10^{-4}$, which is comparable in magnitude to similar studies in 2D and 3D materials [54]. While a larger value for Δ leads to a larger SNE, more work must be done to estimate the size of Δ under relevant experimental conditions.

Figure 6 shows $\alpha_{zy}^x(0,k_y,k_z)$, the k-space contribution to the spin Nernst coefficient such that $\alpha_{zy}^x(k_x=0) = \int d^2k\ \alpha_{zy}^x(0,k_y,k_z)$. Here we clearly see that the net effect is due to an asymmetrical feature in $\alpha_{zy}^x(0,k_y,k_z)$ which is not canceled by contributions elsewhere in the BZ. Furthermore, such an asymmetrical feature exists for general k_x contributions $\alpha_{zy}^x(k_x)$, and not only at $\alpha_{zy}^x(0)$. Since our system obeys $H(k_x) \neq H(-k_x)$, these finite contributions across k_x values do not cancel one another, leading to a finite total SNE $\alpha_{zy}^x = \int dk_x\ \alpha_{zy}^x(k_x)$.

The asymmetrical contribution to the SNE from the locus of points in the third quadrant of the BZ shown in Fig. 6 arise from changes to the band structure induced by symmetry breaking. Most importantly, a curve of near-degeneracy between the highest two bands imparts the large spin Berry curvature required to produce a SNE, and the asymmetrical contribution of that spin Berry curvature arises due to the

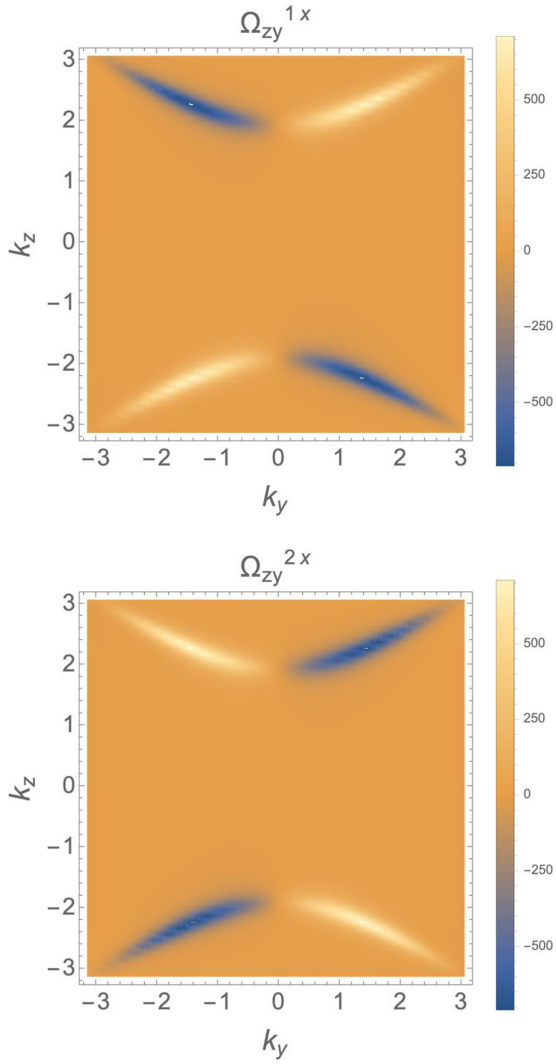

FIG. 5. Magnon spin Berry curvature $\Omega^{nx}_{zy}(0, k_y, k_z)$ for $LaFeO_3$ with applied field $h = (0, 1, 1)$, for $n = 1, 2$, which make the dominant contributions to the spin Berry curvature. Plots for all bands are found in Appendix D.

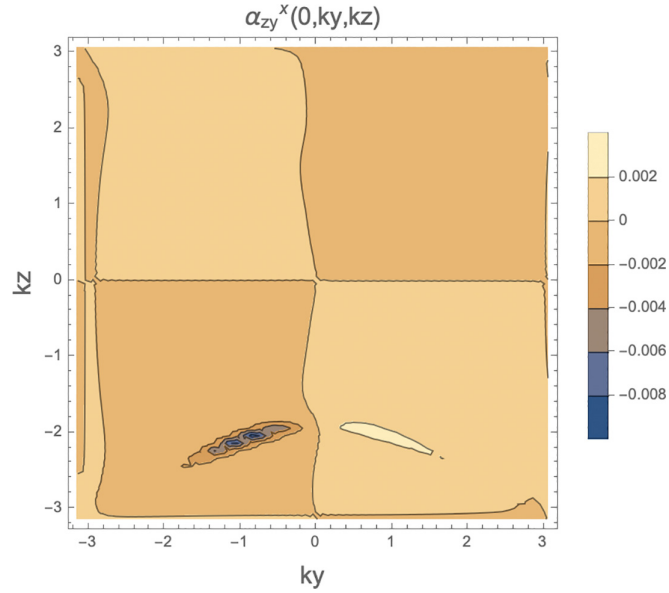

FIG. 6. The total k-space contribution to the SNE. When the spin Berry curvature becomes large through symmetry breaking, an asymmetrical hot spot in contribution arises, which is enough for a finite net SNE.

symmetry breaking. This is shown in the upper panel in Fig. 7. By comparison of Fig. 6 with Fig. 7, one can see the origin of the locus of points with largest spin Berry curvature comes from the regions with the smallest gap. The symmetry of this locus of points is lowered when symmetry is broken.

Finally, we present the temperature dependence of the SNE in the presence of symmetry breaking in Fig. 8. Because the major contributions to the SNE come from the higher-energy bands, we see that higher temperatures lead to a greater SNE due to larger occupation of these bands. It is also important to note that for LFO, $T_N k_B \approx 80$ meV, so this symmetry breaking should lead to an observable SNE even below the critical point.

V. CONCLUSION

In this paper, we have shown that while unstrained/undimerized LFO does not support a SNE that would explain the results of Lin *et al.* [30], under a particular lowering of the bulk symmetry the SNE can become nonzero. This can occur through physical mechanisms such as dimerization along the y and z axes. This effect could explain the anomalous spin transport between LFO and Pt/W observed by Lin *et al.* [30].

We note that our paper also serves a more general purpose for the analysis of transport phenomena in magnetic systems. We have introduced a framework for relaxing cancellation effects at the level of generalized Berry curvature which usually result in the vanishing of nontrivial currents. In our case, this cancellation was due to inversion symmetries in the spin Berry curvature. We systematically analyzed the necessary and sufficient conditions for lowering such a symmetry of a BdG Hamiltonian—the result Eq. (24) is general.

Our paper paves the way for further research into spin transport in $LaFeO_3$. A particularly important question that remains is to identify under what conditions dimerization would be achieved in $LaFeO_3$, so the SNE would manifest via the particular mechanism we discussed above. Possible mechanisms generally include Peierls dimerization through spin-phonon coupling [60] and magnetic frustration, such as occurs in the well-known Majumdar-Gosh model [61]. Possible material realizations of dimerized magnetic states are $KCuCl_3$ and $TlCuCl_3$ [62] and $SrCu_2(BO_3)_2$ [63].

In our paper, we have neglected effects that could arise due to the interface with Pt; see, for example, Ref. [64]. Lattice relaxation effects due to the interface as well as couplings between spins in LFO and itinerant electrons in Pt could play important roles in the symmetry breaking we have discussed. Strain may be yet another way that Eq. (24) might be realized, thus breaking inversion symmetry at the level of bosons similarly to the effect of strain in Weyl semimetals [65].

Another question is whether interesting phenomena might arise in the context of other forms of Eq. (24) and, in particu-

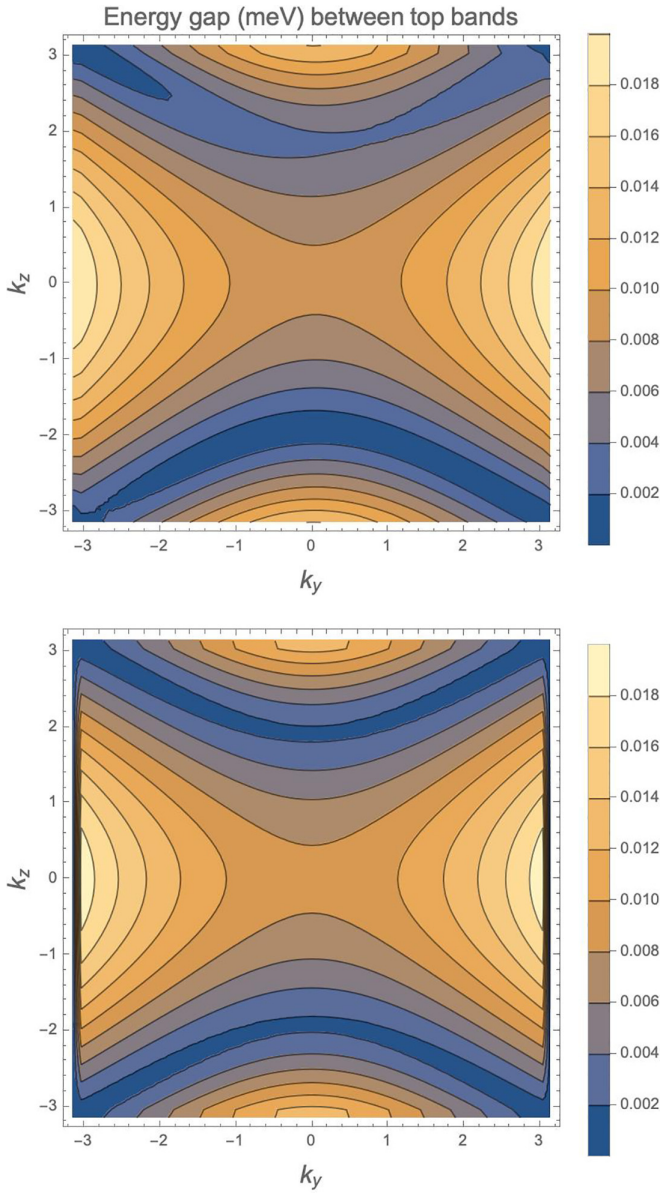

FIG. 7. Energy gap between two highest bands. Top: The difference between the energies of the top two bands after symmetry breaking. Bottom: The same quantity computed before symmetry breaking.

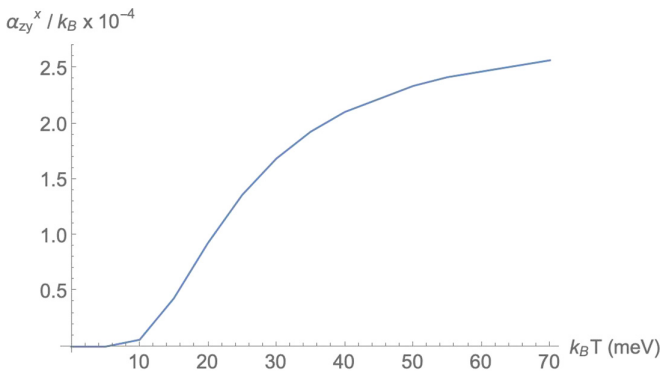

FIG. 8. SNE as a function of temperature, for $\Delta/J = 0.1$.

lar, whether any such Hamiltonian might arise by accounting for magnon-phonon coupling in bulk $LaFeO_3$ and related materials. Of course, when discussing interfacial spin transport, the dynamics at the interface can play an important role in addition to the bulk properties we have focused on in this paper. Further research might characterize, for example, the magnon dynamics at the interface, which would provide a more complete story regarding the observed magnetothermovoltage in $LaFeO_3$/Pt.

Having derived a mechanism by which a finite SNE may arise in systems where it is disallowed by symmetry, our paper also opens the possibility of engineering transport effects in magnetic systems. For example, this might be accomplished by inducing dimerization as we describe above.

ACKNOWLEDGMENTS

We acknowledge support from NSF No. DMR-2114825, DOE Award No. DE-SC0022168, and the Alexander von Humboldt Foundation. W.R. acknowledges support from the U.S. Department of Defense through the NDSEG Fellowship.

APPENDIX A: BOGOLIUBOV-DE GENNES FOURIER TRANSFORM AND PARAUNITARY TRANSFORMATIONS

Expanding around the classical spin configuration above, our Hamiltonian takes the form

$$H \approx \sum_{\vec{r},\vec{\delta}} \psi^{\dagger}(\vec{r}) H_{\vec{\delta}} \psi(\vec{r}+\vec{\delta}), \tag{A1}$$

where $\vec{r}$ labels the lattice site and $\vec{\delta}$ are the relevant nearest- and next-nearest-neighbor separation vectors. Here, $\psi(\vec{r})$ is a Nambu spinor, given by

$$\psi(\vec{r}) = \begin{pmatrix} a_1(\vec{r}) \\ a_2(\vec{r}) \\ a_3(\vec{r}) \\ a_4(\vec{r}) \\ a_1^{\dagger}(\vec{r}) \\ a_2^{\dagger}(\vec{r}) \\ a_3^{\dagger}(\vec{r}) \\ a_4^{\dagger}(\vec{r}) \end{pmatrix}. \tag{A2}$$

We have eliminated linear bosonic terms by expanding around the energetic minimum, and we have dropped constants as well as interaction terms of three bosonic operators an higher, consistent with a Taylor expansion in $(1/S)$ of the Holstein-Primakov transformation.

If we let $\vec{x}_i$ be the separation between sublattices 1 and i, then we can define a Fourier transformation:

$$a_i(\vec{r}) = \frac{1}{\sqrt{N}} \sum_{\vec{k}} e^{i\vec{k}\cdot(\vec{r}+\vec{x}_i)} a(\vec{k}). \tag{A3}$$

Performing this Fourier transform results in the form

$$H = \sum_{k} \psi_k^{\dagger} H_k \psi_k, \tag{A4}$$

where the k-space Nambu spinors are given by

$$\psi_k = \begin{pmatrix} a_1(\vec{k}) \\ a_2(\vec{k}) \\ a_3(\vec{k}) \\ a_4(\vec{k}) \\ a_1^\dagger(-\vec{k}) \\ a_2^\dagger(-\vec{k}) \\ a_3^\dagger(-\vec{k}) \\ a_4^\dagger(-\vec{k}) \end{pmatrix}.$$

The minus sign in the creation operators is inherited from the definition of the Fourier transform at the level of the bosonic operators,

$$\psi(\vec{r}) = \frac{1}{\sqrt{N}} \sum_k e^{i\vec{k}\cdot\vec{r}} \begin{pmatrix} a_1(\vec{k}) \\ e^{i\vec{k}\cdot\vec{x}_2} a_2(\vec{k}) \\ e^{i\vec{k}\cdot\vec{x}_3} a_3(\vec{k}) \\ e^{i\vec{k}\cdot\vec{x}_4} a_4(\vec{k}) \\ a_1^\dagger(-\vec{k}) \\ e^{i\vec{k}\cdot\vec{x}_2} a_2^\dagger(-\vec{k}) \\ e^{i\vec{k}\cdot\vec{x}_3} a_3^\dagger(-\vec{k}) \\ e^{i\vec{k}\cdot\vec{x}_4} a_4^\dagger(-\vec{k}) \end{pmatrix} = \frac{1}{\sqrt{N}} \sum_k e^{i\vec{k}\cdot\vec{r}} U_k \psi_k, \tag{A5}$$

where U_k collects the sublattice separation phases, so

$$U_k = \begin{pmatrix} 1 & 0 & 0 & 0 & 0 & 0 & 0 & 0 \\ 0 & e^{i\vec{k}\cdot\vec{x}_2} & 0 & 0 & 0 & 0 & 0 & 0 \\ 0 & 0 & e^{i\vec{k}\cdot\vec{x}_3} & 0 & 0 & 0 & 0 & 0 \\ 0 & 0 & 0 & e^{i\vec{k}\cdot\vec{x}_4} & 0 & 0 & 0 & 0 \\ 0 & 0 & 0 & 0 & 1 & 0 & 0 & 0 \\ 0 & 0 & 0 & 0 & 0 & e^{i\vec{k}\cdot\vec{x}_2} & 0 & 0 \\ 0 & 0 & 0 & 0 & 0 & 0 & e^{i\vec{k}\cdot\vec{x}_3} & 0 \\ 0 & 0 & 0 & 0 & 0 & 0 & 0 & e^{i\vec{k}\cdot\vec{x}_4} \end{pmatrix}. \tag{A6}$$

This formalism also allows us to relate the position- and momentum-space Hamiltonian matrices $H_{\vec{\delta}}$ and H_k. By applying Eq. (A5) directly to Eq. (A1), we find that

$$H_k = \sum_\delta U_k^\dagger H_{\vec{\delta}} U_k. \tag{A7}$$

Thus, solving the Fourier transformed problem amounts to diagonalizing the matrix H_k. However, care must be taken to ensure that the transformation T_k such that $T_k^\dagger H_k T_k = \Lambda_k$ (with Λ_k diagonal) also preserves the bosonic commutation relations

$$[\psi_k, \psi_k^\dagger] = \begin{pmatrix} I_4 & 0 \\ 0 & -I_4 \end{pmatrix} \equiv \eta, \tag{A8}$$

so in the diagonal problem $H = \sum_k \Lambda_k \gamma_k^\dagger \gamma_k$, the operators $\gamma_k^\dagger \gamma_k$ are number operators. It turns out that for this to be the case, T_k must be a paraunitary transformation [9,50,51], which means

$$T_k \eta T_k^\dagger = \eta. \tag{A9}$$

Equation (A9) implies that rather than diagonalize H_k via similarity transformation in the usual way, the eigenvalue problem we should solve to obtain the magnon dispersion is

$$\sigma_3 H_k |\psi_k^n\rangle = E_k^n |\psi_k^n\rangle. \tag{A10}$$

The kets $|\psi_k^n\rangle$ that solve the eigenproblem are columns of T_k, and from paraunitarity they inherit the normalization condition

$$\langle \psi_k^m | \eta | \psi_k^n \rangle = \eta_{mn}. \tag{A11}$$

We call solutions with norm 1 particle bands and those with norm -1 hole bands. Equivalently, the bands with positive eigenenergies (norm 1) are physical particle bands and the bands with opposite sign are the hole partners.

APPENDIX B: THE PARAUNITARY EIGENVALUE PROBLEM IN BDG FORMALISM

Consider the general BdG Hamiltonian

$$H = \sum_k \psi_k^\dagger H_k \psi_k, \tag{B1}$$

where $\psi_k^\dagger = (a_{k1}^\dagger, ..., a_{kN}^\dagger, a_{-k1}, ..., a_{-kN})$. The operators a can be bosonic or fermionic. We can package the commutation relations in terms of elements of ψ in each case.

For fermions, we have

$$\{\psi_{ki}, \psi_{kj}^\dagger\} = I_{ij}, \tag{B2}$$

while for bosons we find

$$[\psi_{ki}, \psi_{kj}^\dagger] = \eta_{ij}, \tag{B3}$$

where η is diagonal with $+1$ for the upper N elements and -1 for the lower.

We seek a form

$$H = \sum_k \tilde{\psi}_k^\dagger \tilde{H}_k \tilde{\psi}_k,$$

in which $\tilde{H}_k$ is diagonal. However, the structure of (B1), specifically with the presence of terms that don't conserve particle number, means that when we diagonalize H_k in the usual way, creation and annihilation operators can mix in such a way that the objects we would interpret as quasiparticles don't obey the original fermionic or bosonic commutation relations. Put another way, we don't know whether we will still be able to interpret the diagonalizing basis $\tilde{\psi}$ as creation and annihilation operators. There is at least no guarantee they'll be the usual second quantized operators, in which case the diagonal form will not be useful.

So, we seek a transformation that not only gives a diagonal $\tilde{H}_k$ but that also preserves (B2) in the fermionic case and (B3) in the bosonic case. Defining this transformation so

$$T_k^{-1} \psi_k = \tilde{\psi}_k, \tag{B4}$$

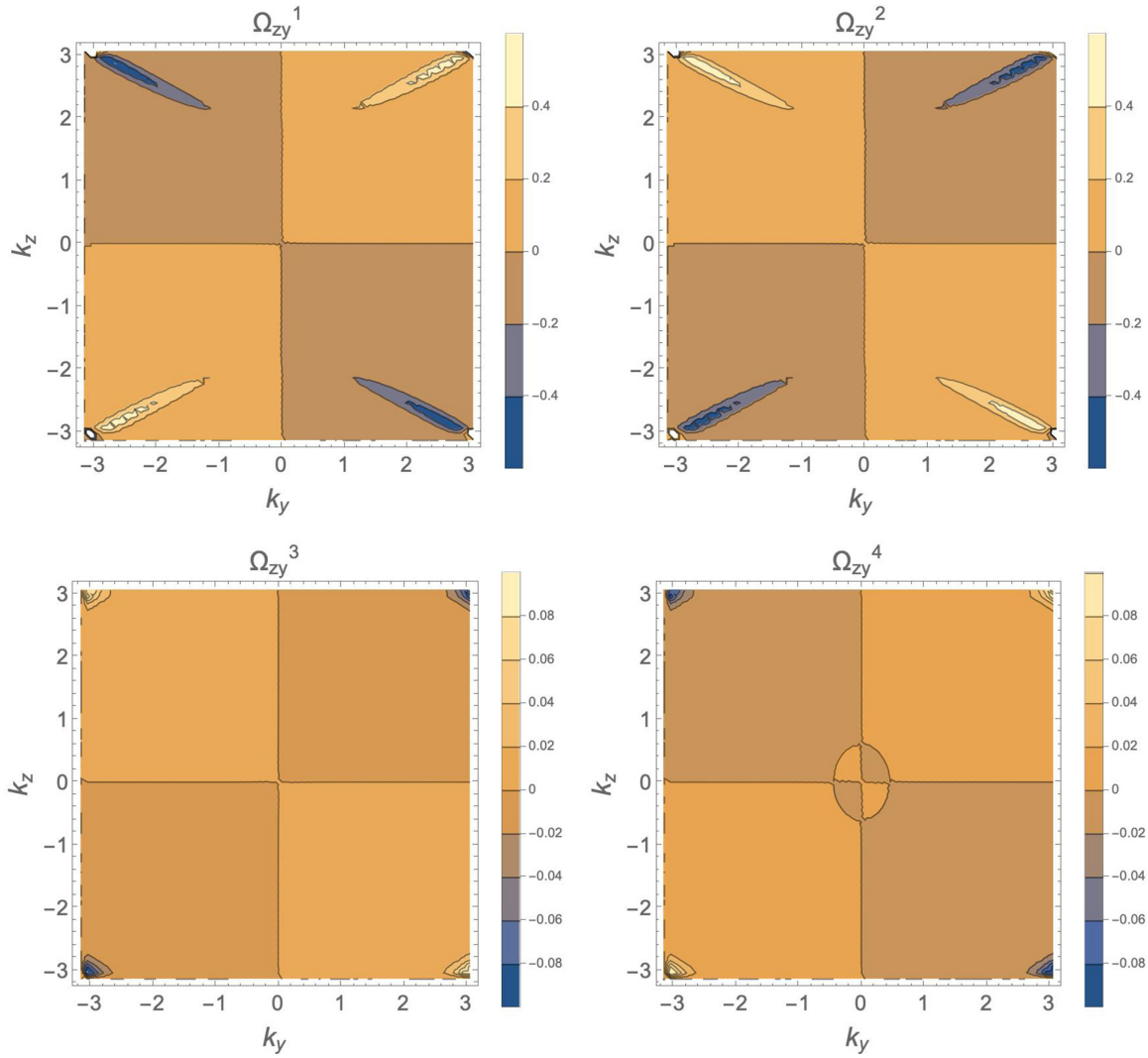

FIG. 9. Magnon Berry curvature $\Omega^n_{zy}(0, k_y, k_z)$ for LFO with applied field $h = (0, 1, 1)$ for all bands.

so the Hamiltonian can be rewritten as

$$H = \sum_k \psi_k^\dagger (T_k^\dagger)^{-1} T_k^\dagger H_k T_k T_k^{-1} \psi_k = \sum_k \tilde{\psi}_k^\dagger T_k^\dagger H_k T_k, \quad \text{(B5)}$$

we can look for T such that the desired commutation relations are preserved and for which $T_k^\dagger H_k T_k = \tilde{H}_k$ is diagonal.

It turns out that the commutation condition places different constraints on T. For fermions, the condition is actually that T is unitary. This means that in that case we can just diagonalize as usual. To see this, we can just look at what happens when we enforce

$$\{\tilde{\psi}_{ki}, \tilde{\psi}_{kj}^\dagger\} = I_{ij}$$

for the transformed basis. Starting from (B2), we can rewrite the relation in index notation using the following steps (where the k dependence has been suppressed for clarity):

$$\begin{aligned}
\psi_i \psi_j^\dagger + \psi_j^\dagger \psi_i &= I_{ij}, \\
T_{im} \tilde{\psi}_m \tilde{\psi}_n^\dagger T_{nj}^\dagger + \tilde{\psi}_n^\dagger T_{nj}^\dagger T_{im} \tilde{\psi}_m &= I_{ij}, \\
T_{ri}^{-1} T_{im} \tilde{\psi}_m \tilde{\psi}_n^\dagger T_{nj}^\dagger (T^\dagger)_{jp}^{-1} + \tilde{\psi}_n^\dagger T_{nj}^\dagger (T^\dagger)_{jp}^{-1} T_{ri}^{-1} T_{im} \tilde{\psi}_m & \\
= T_{ri}^{-1} I_{ij} (T^\dagger)_{jp}^{-1}, & \\
\tilde{\psi}_r \tilde{\psi}_p^\dagger + \tilde{\psi}_p^\dagger \tilde{\psi}_r = T_{ri}^{-1} (T^\dagger)_{ip}^{-1}. & \quad \text{(B6)}
\end{aligned}$$

If we enforce the anticommutation relation for the $\tilde{\psi}$ basis, this is the condition that

$$T_k^\dagger T_k = I.$$

That is, for fermions, T_k is unitary. Therefore, $\tilde{H}_k$ is truly just the diagonalized form of H_k.

For bosons, the same steps give

$$\begin{aligned}
\psi_i \psi_j^\dagger - \psi_j^\dagger \psi_i &= \eta_{ij}, \\
T_{im} \tilde{\psi}_m \tilde{\psi}_n^\dagger T_{nj}^\dagger - \tilde{\psi}_n^\dagger T_{nj}^\dagger T_{im} \tilde{\psi}_m &= \eta_{ij}, \\
T_{ri}^{-1} T_{im} \tilde{\psi}_m \tilde{\psi}_n^\dagger T_{nj}^\dagger (T^\dagger)_{jp}^{-1} - \tilde{\psi}_n^\dagger T_{nj}^\dagger (T^\dagger)_{jp}^{-1} T_{ri}^{-1} T_{im} \tilde{\psi}_m & \\
= T_{ri}^{-1} \eta_{ij} (T^\dagger)_{jp}^{-1}, & \\
\tilde{\psi}_r \tilde{\psi}_p^\dagger - \tilde{\psi}_p^\dagger \tilde{\psi}_r = T_{ri}^{-1} \eta_{ij} (T^\dagger)_{jp}^{-1}. & \quad \text{(B7)}
\end{aligned}$$

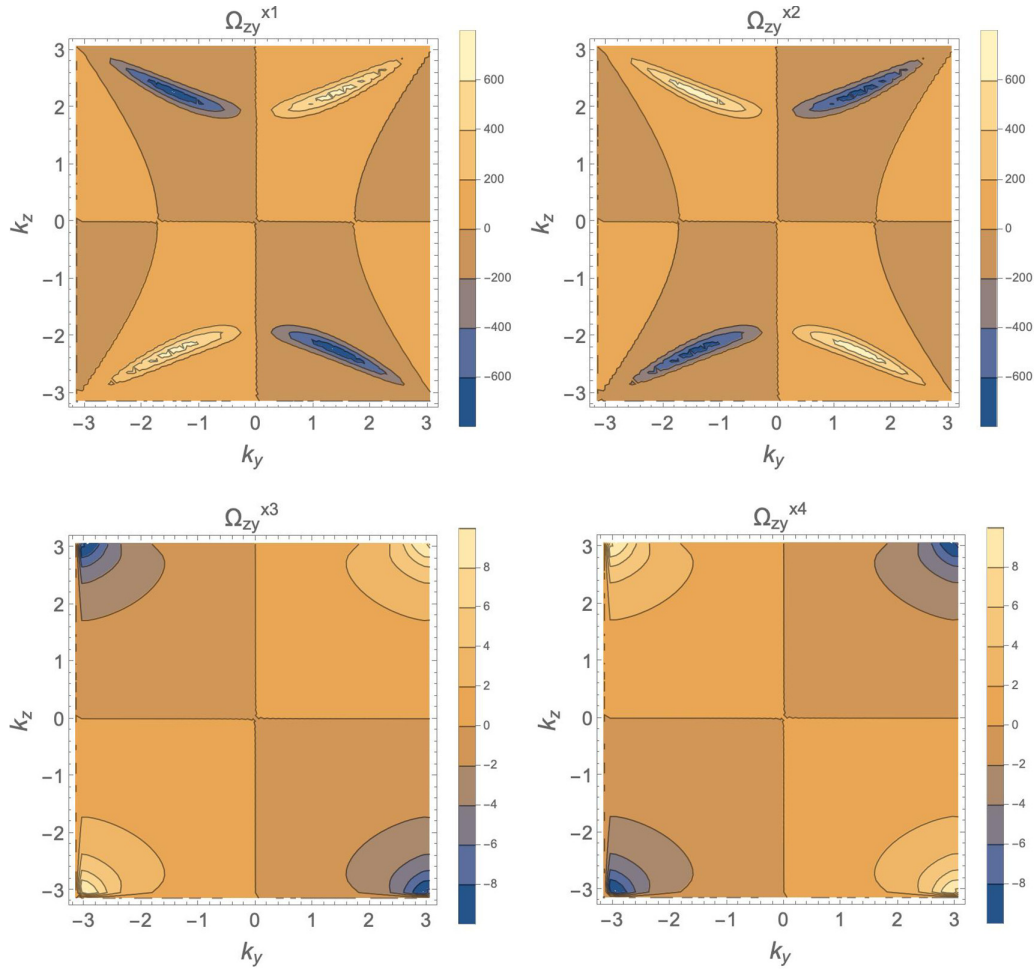

FIG. 10. Magnon spin Berry curvature $\Omega_{zy}^{nx}(0, k_y, k_z)$ for LFO with applied field $h = (0, 1, 1)$.

Enforcing (B3) now gives

$$\eta_{rp} = T_{ri}^{-1}\eta_{ij}(T^{\dagger})_{jp}^{-1} \tag{B8}$$

or just

$$\eta = T_k^{-1}\eta(T_k^{\dagger})^{-1}. \tag{B9}$$

This is the origin of the paraunitary condition $\eta = T_k\eta T_k^{\dagger}$. This condition on T_k is required so $\tilde{H}_k$ (in this case, not the diagonalized form of H_k) is diagonal, while the transformed operators still make physical sense as corresponding to bosons.

We've seen that for the bosonic BdG system we can't just diagonalize as usual but instead need to employ a paraunitary transformation. The eigenvalue problem is correspondingly modified, so

$$T_k^{\dagger}H_kT_k = \begin{bmatrix} E_k & 0 \\ 0 & E_{-k} \end{bmatrix}, \tag{B10}$$

where for $N > 1$, the E_k are themselves diagonal matrices. Note that $\eta T_k^{\dagger}\eta = T_k^{-1}$. This allows us to rewrite (B10) as

$$\eta T_k^{\dagger}\eta\eta H_kT_k = T_k^{-1}\eta H_kT_k = \begin{bmatrix} E_k & 0 \\ 0 & -E_{-k} \end{bmatrix}. \tag{B11}$$

This tells us that the relevant similarity transformation is of the non-Hermitian matrix ηH_k. The corresponding eigenvalue problem is obtained by multiplying both sides of (B11) on the left by T_k to give

$$\eta H_kT_k = T_k\begin{bmatrix} E_k & 0 \\ 0 & -E_{-k} \end{bmatrix}. \tag{B12}$$

We can read this as comprising $2N$ eigenvalue problems, where the columns of T_k are the eigenvectors of ηH_k. This is why we find definitions of topological magnon quantities that involve projections of T_k—the paraunitary matrix encodes the eigenstates of the physical problem, i.e., the true quasiparticles.

APPENDIX C: GENERALITY OF SYMMETRY-BREAKING TERM

Here we derive the most general form of a symmetry-breaking term that will produce a BdG Hamiltonian with terms like Eq. (23). We can look for nearest-neighbor couplings, as these will be the strongest; these couple bosons from neighboring sublattices. Writing the operator content explicitly, and first focusing on pairing terms with we denote

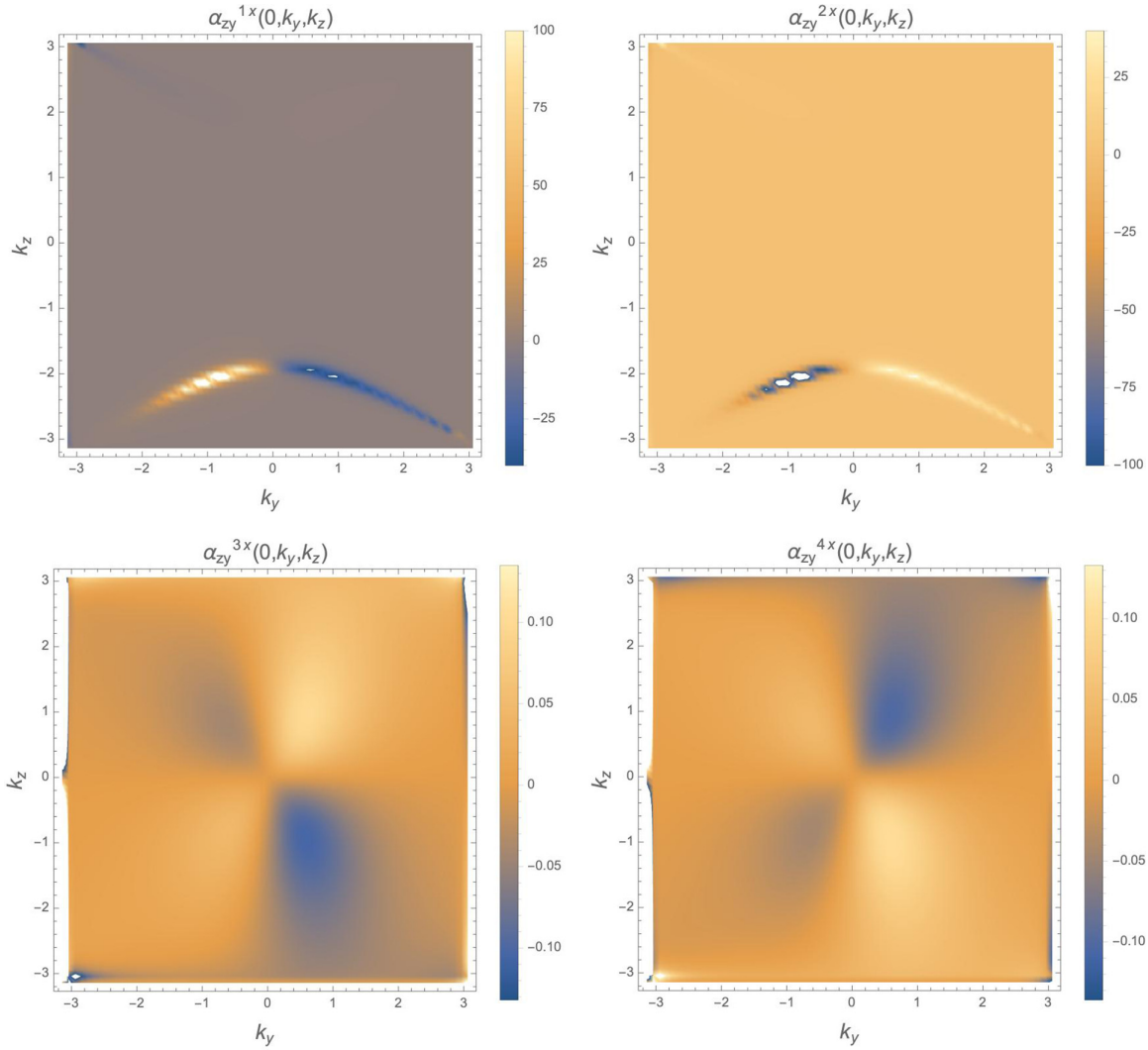

FIG. 11. The contribution to the SNE from each band for $k_BT = 10$. This is a low enough temperature that band 2 contributes more heavily than band 1, creating a negative SNE.

with subscript B, we can therefore ask about terms such as

$$H^B_\Delta = \frac{\Delta^B}{2}\sum_k [\sin(kl)b_{-k}a_k - \sin(kl)a_{-k}b_k] + \text{H.c.}, \quad \text{(C1)}$$

where we restrict to one dimension for now for simplicity, since the argument will run the same for both k_z and k_y. Here Δ^B is an arbitrary, complex constant. The minus signs result from insisting that the ansatz be particle-hole symmetric. Transforming the first term to direct-lattice bosons gives

$$\sum_k \sin(kl)b_{-k}a_k = \frac{1}{2i}\sum_j (a_j b_{j-x_b-l} - a_j b_{j-x_b+l}),$$

where x_b is the direct-lattice separation between the a and b sublattices. From this, we see an immediate restriction on the possible values of l, stemming from the fact that the index of the b bosons must be a lattice vector; $l + x_b$ and $l - x_b$ must therefore also be lattice vectors. Here x_b is half the length of a unit cell along the direction of interest, and furthermore we wish to restrict to nearest-neighbor couplings. Therefore, the only consistent choices are $l = \pm x_b$. The choice of sign is equivalent to a choice of sign of the overall term, so without loss of generality we can consider the choice $l = x_b$.

Transforming to spin operators via an inverse Holstein-Primakov transformation, we find that the inversion-breaking term must have the form

$$\begin{aligned} H^B_\Delta &= \frac{\Delta^B_R}{2i}\sum_j [\tilde{S}^+_{aj}\tilde{S}^+_{bj-1} - \tilde{S}^+_{aj}\tilde{S}^+_{bj} - \tilde{S}^-_{aj}\tilde{S}^-_{bj-1} + \tilde{S}^-_{aj}\tilde{S}^-_{bj}] \\ &\quad + \frac{\Delta^B_I}{2}\sum_j [\tilde{S}^+_{aj}\tilde{S}^+_{bj-1} - \tilde{S}^+_{aj}\tilde{S}^+_{bj} + \tilde{S}^-_{aj}\tilde{S}^-_{bj-1} - \tilde{S}^-_{aj}\tilde{S}^-_{bj}] \\ &= \Delta^B_R \sum_j \left[\tilde{S}^y_{aj}\tilde{S}^x_{bj-1} - \tilde{S}^y_{aj}\tilde{S}^x_{bj} + \tilde{S}^x_{aj}\tilde{S}^y_{bj-1} - \tilde{S}^x_{aj}\tilde{S}^y_{bj}\right] \\ &\quad + \Delta^B_I \sum_j \left[\tilde{S}^x_{aj}\tilde{S}^x_{bj-1} - \tilde{S}^x_{aj}\tilde{S}^x_{bj} - \tilde{S}^y_{aj}\tilde{S}^y_{bj-1} + \tilde{S}^y_{aj}\tilde{S}^y_{bj}\right], \end{aligned} \quad \text{(C2)}$$

where $\tilde{S}^\alpha$ is a spin operator written in the locally rotated frame. Here we have defined the real numbers Δ^B_R and Δ^B_I in $\Delta^B = \Delta^B_R + i\Delta^B_I$.

A similar analysis can be done for nonpairing terms, such as

$$H_\Delta^A = \frac{\Delta^A}{2}\sum_k [\sin(kl)a_k^\dagger b_k - \sin(kl)b_{-k}a_{-k}^\dagger] + \text{H.c.}$$

In this case, we find the same restriction on l, resulting in possible inversion-breaking terms of the form

$$H_\Delta^A = \Delta_R^A \sum_j \left[\tilde{S}_{aj}^x \tilde{S}_{bj-1}^y - \tilde{S}_{aj}^y \tilde{S}_{bj-1}^x - \tilde{S}_{aj}^x \tilde{S}_{bj}^y + \tilde{S}_{aj}^y \tilde{S}_{bj}^x\right] + \Delta_I^A \sum_j \left[\tilde{S}_{aj}^x \tilde{S}_{bj-1}^x + \tilde{S}_{aj}^y \tilde{S}_{bj-1}^y - \tilde{S}_{aj}^x \tilde{S}_{bj}^x - \tilde{S}_{aj}^y \tilde{S}_{bj}^y\right]. \tag{C3}$$

Thus, the form of inversion-breaking terms is quite restricted to some linear combination $H_\Delta = H_\Delta^A + H_\Delta^B$. Letting $\Gamma^{xx} = \Delta_I^A + \Delta_I^B$, $\Gamma^{yy} = \Delta_I^A - \Delta_I^B$, $\Gamma^{xy} = \Delta_R^A + \Delta_R^B$, and $\Gamma^{yx} = -\Delta_I^A + \Delta_I^B$, we can write the term H_Δ as

$$H_\Delta = \sum_j \Gamma^{\alpha\beta}\left(S_{aj}^\alpha S_{bj-1}^\beta - S_{aj}^\alpha S_{bj}^\beta\right), \tag{C4}$$

thus proving that Eq. (24) is the most general term that breaks inversion symmetry along the direction indexed by j. Notably, we find that any choice of couplings $\Gamma^{\alpha\beta}$ will produce symmetry breaking; the key component is the minus sign between the terms inside and outside the unit cell. As shown in the main text, couplings involving z components do not contribute to the lowest-order Holstein-Primakov expansion and are therefore neglected.

APPENDIX D: ADDITIONAL PLOTS

Here we present additional plots to supplement the discussion in the main text. Figure 9 displays the band Berry curvature $\Omega_{zy}^n(0, k_y, k_z)$ and Fig. 10 displays the spin Berry curvature $\Omega_{zy}^{nx}(0, k_y, k_z)$.

In the main text, we considered the net contribution $\alpha_{zy}^x(k_x)$ from all bands. We can also look at the contributions from individual (particle) bands, such that $\alpha_{zy}^x = \sum_n \alpha_{zy}^{nx}$. Here we find that the asymmetrical feature in Fig. 6 is contributed by the two higher bands, suggesting that, to see the effect, the temperature must be high enough to allow occupation of these bands. This is depicted in Fig. 11.

[1] I. Žutić, J. Fabian, and S. Das Sarma, Spintronics: Fundamentals and applications, Rev. Mod. Phys. **76**, 323 (2004).

[2] S. D. Bader and S. S. P. Parkin, Spintronics, Annu. Rev. Condens. Matter Phys. **1**, 71 (2010).

[3] G. E. W. Bauer, E. Saitoh, and B. J. V. Wees, Spin caloritronics, Nat. Mater. **11**, 391 (2012).

[4] H. Yu, S. D. Brechet, and J.-P. Ansermet, Spin caloritronics, origin and outlook, Phys. Lett. A **381**, 825 (2017).

[5] D. Lujan, J. Choe, M. Rodriguez-Vega, Z. Ye, A. Leonardo, T. N. Nunley, L.-J. Chang, S.-F. Lee, J. Yan, G. A. Fiete, R. He, and X. Li, Magnons and magnetic fluctuations in atomically thin $MnBi_2Te_4$, Nat. Commun. **13**, 2527 (2022).

[6] H. Y. Yuan, Y. Cao, A. Kamra, R. A. Duine, and P. Yan, Quantum magnonics: When magnon spintronics meets quantum information science, Phys. Rep. **965**, 1 (2022).

[7] A. Barman, G. Gubbiotti, S. Ladak, A. O. Adeyeye, M. Krawczyk, J. Gräfe, C. Adelmann, S. Cotofana, A. Naeemi, V. I. Vasyuchka, B. Hillebrands, S. A. Nikitov, H. Yu, D. Grundler, A. V. Sadovnikov, A. A. Grachev, S. E. Sheshukova, J.-Y. Duquesne, M. Marangolo, G. Csaba *et al.*, The 2021 magnonics roadmap, J. Phys.: Condens. Matter **33**, 413001 (2021).

[8] V. V. Kruglyak, S. O. Demokritov, and D. Grundler, Magnonics, J. Phys. D **43**, 264001 (2010).

[9] P. A. McClarty, Topological magnons: A review, Annu. Rev. Condens. Matter Phys. **13**, 171 (2022).

[10] M. dos Santos Dias, N. Biniskos, F. J. dos Santos, K. Schmalzl, J. Persson, F. Bourdarot, N. Marzari, S. Blügel, T. Brückel, and S. Lounis, Topological magnons driven by the Dzyaloshinskii-Moriya interaction in the centrosymmetric ferromagnet Mn_5Ge_3, Nat. Commun. **14**, 7321 (2023).

[11] R. Matsumoto, R. Shindou, and S. Murakami, Thermal Hall effect of magnons in magnets with dipolar interaction, Phys. Rev. B **89**, 054420 (2014).

[12] A. A. Kovalev, V. A. Zyuzin, and B. Li, Pumping of magnons in a Dzyaloshinskii-Moriya ferromagnet, Phys. Rev. B **95**, 165106 (2017).

[13] T. Qin, Q. Niu, and J. Shi, Energy magnetization and the thermal Hall effect, Phys. Rev. Lett. **107**, 236601 (2011).

[14] Y. Onose, T. Ideue, H. Katsura, Y. Shiomi, N. Nagaosa, and Y. Tokura, Observation of the magnon Hall effect, Science **329**, 297 (2010).

[15] H. Katsura, N. Nagaosa, and P. A. Lee, Theory of the thermal Hall effect in quantum magnets, Phys. Rev. Lett. **104**, 066403 (2010).

[16] R. Matsumoto and S. Murakami, Theoretical prediction of a rotating magnon wave packet in ferromagnets, Phys. Rev. Lett. **106**, 197202 (2011).

[17] T. Ideue, Y. Onose, H. Katsura, Y. Shiomi, S. Ishiwata, N. Nagaosa, and Y. Tokura, Effect of lattice geometry on magnon Hall effect in ferromagnetic insulators, Phys. Rev. B **85**, 134411 (2012).

[18] L. Zhang, J. Ren, J.-S. Wang, and B. Li, Topological magnon insulator in insulating ferromagnet, Phys. Rev. B **87**, 144101 (2013).

[19] A. Mook, J. Henk, and I. Mertig, Magnon Hall effect and topology in kagome lattices: A theoretical investigation, Phys. Rev. B **89**, 134409 (2014).

[20] P. Laurell and G. A. Fiete, Magnon thermal Hall effect in kagome antiferromagnets with Dzyaloshinskii-Moriya interactions, Phys. Rev. B **98**, 094419 (2018).

[21] W. O. Wang, J. K. Ding, B. Moritz, E. W. Huang, and T. P. Devereaux, Magnon heat transport in a two-dimensional Mott insulator, Phys. Rev. B **105**, L161103 (2022).

[22] B. Zare Rameshti, S. Viola Kusminskiy, J. A. Haigh, K. Usami, D. Lachance-Quirion, Y. Nakamura, C.-M. Hu, H. X. Tang, G. E. W. Bauer, and Y. M. Blanter, Cavity magnonics, Phys. Rep. **979**, 1 (2022).

[23] K. Park, H. Sim, J. C. Leiner, Y. Yoshida, J. Jeong, S. I. Yano, J. Gardner, P. Bourges, M. Klicpera, V. Sechovský, M. Boehm, and J.-G. Park, Low-energy spin dynamics of orthoferrites $AFeO_3$ (A = Y, La, Bi), J. Phys.: Condens. Matter **30**, 235802 (2018).

[24] T. Jia, Z. Zeng, H. Q. Lin, Y. Duan, and P. Ohodnicki, First-principles study on the electronic, optical and thermodynamic properties of ABO_3 (A = La,Sr, B = Fe,Co) perovskites, RSC Adv. **7**, 38798 (2017).

[25] M. Zhu, J. Lanier, S. P. Genlik, F. J. G, V. Barbosa, P. Woodward, M. Ghazisaeidi, F. Yang, and J. Hwang, Strain-induced Ferromagnetism at $LaFeO_3/SrTiO_3$ Interface, Microsc. Microanal. **29**, 1637 (2023).

[26] E. Bousquet and A. Cano, Non-collinear magnetism in multiferroic perovskites, J. Phys.: Condens. Matter **28**, 123001 (2016).

[27] J.-S. Zhou, L. G. Marshall, Z.-Y. Li, X. Li, and J.-M. He, Weak ferromagnetism in perovskite oxides, Phys. Rev. B **102**, 104420 (2020).

[28] I. Dzyaloshinsky, A thermodynamic theory of "weak" ferromagnetism of antiferromagnetics, J. Phys. Chem. Solids **4**, 241 (1958).

[29] T. Moriya, Anisotropic superexchange interaction and weak ferromagnetism, Phys. Rev. **120**, 91 (1960).

[30] W. Lin, J. He, B. Ma, M. Matzelle, J. Xu, J. Freeland, Y. Choi, D. Haskel, B. Barbiellini, A. Bansil, G. A. Fiete, J. Zhou, and C. L. Chien, Evidence for spin swapping in an antiferromagnet, Nat. Phys. **18**, 800 (2022).

[31] B. Li, S. Sandhoefner, and A. A. Kovalev, Intrinsic spin Nernst effect of magnons in a noncollinear antiferromagnet, Phys. Rev. Res. **2**, 013079 (2020).

[32] V. A. Zyuzin and A. A. Kovalev, Magnon spin Nernst effect in antiferromagnets, Phys. Rev. Lett. **117**, 217203 (2016).

[33] A. A. Kovalev and V. Zyuzin, Spin torque and Nernst effects in Dzyaloshinskii-Moriya ferromagnets, Phys. Rev. B **93**, 161106(R) (2016).

[34] R. Cheng, S. Okamoto, and D. Xiao, Spin nernst effect of magnons in collinear antiferromagnets, Phys. Rev. Lett. **117**, 217202 (2016).

[35] H. Zhang and R. Cheng, A perspective on magnon spin Nernst effect in antiferromagnets, Appl. Phys. Lett. **120**, 090502 (2022).

[36] H. Kondo and Y. Akagi, Nonlinear magnon spin Nernst effect in antiferromagnets and strain-tunable pure spin current, Phys. Rev. Res. **4**, 013186 (2022).

[37] B. He, C. Şahin, S. R. Boona, B. C. Sales, Y. Pan, C. Felser, M. E. Flatté, and J. P. Heremans, Large magnon-induced anomalous Nernst conductivity in single-crystal MnBi, Joule **5**, 3057 (2021).

[38] B. Ma and G. A. Fiete, Intrinsic magnon nernst effect in pyrochlore iridate thin films, Phys. Rev. B **104**, 174410 (2021).

[39] E. Saitoh, M. Ueda, H. Miyajima, and G. Tatara, Conversion of spin current into charge current at room temperature: Inverse spin-Hall effect, Appl. Phys. Lett. **88**, 182509 (2006).

[40] M. V. Costache, M. Sladkov, S. M. Watts, C. H. van der Wal, and B. J. van Wees, Electrical detection of spin pumping due to the precessing magnetization of a single ferromagnet, Phys. Rev. Lett. **97**, 216603 (2006).

[41] T. Kimura, Y. Otani, T. Sato, S. Takahashi, and S. Maekawa, Room-temperature reversible spin Hall effect, Phys. Rev. Lett. **98**, 156601 (2007).

[42] K. Uchida, M. Ishida, T. Kikkawa, A. Kirihara, T. Murakami, and E. Saitoh, Longitudinal spin Seebeck effect: From fundamentals to applications, J. Phys.: Condens. Matter **26**, 343202 (2014).

[43] P. V. Coutinho, F. Cunha, and P. Barrozo, Structural, vibrational and magnetic properties of the orthoferrites $LaFeO_3$ and $YFeO_3$: A comparative study, Solid State Commun. **252**, 59 (2017).

[44] R. L. White, Review of recent work on the magnetic and spectroscopic properties of the rare-earth orthoferrites, J. Appl. Phys. **40**, 1061 (1969).

[45] D. Treves, Magnetic studies of some orthoferrites, Phys. Rev. **125**, 1843 (1962).

[46] W. C. Koehler and E. O. Wollan, Neutron-diffraction study of the magnetic properties of perovskite-like compounds LaBO3, J. Phys. Chem. Solids **2**, 100 (1957).

[47] T. Holstein and H. Primakoff, Field dependence of the intrinsic domain magnetization of a ferromagnet, Phys. Rev. **58**, 1098 (1940).

[48] B. D. Simons and A. Altland, *Condensed Matter Field Theory* (Cambridge University Press, Cambridge, UK, 2010).

[49] A. G. D. Maestro and M. J. P. Gingras, Quantum spin fluctuations in the dipolar Heisenberg-like rare earth pyrochlores, J. Phys.: Condens. Matter **16**, 3339 (2004).

[50] H. Kondo, Y. Akagi, and H. Katsura, Non-Hermiticity and topological invariants of magnon Bogoliubov–de Gennes systems, Prog. Theor. Exp. Phys. **2020**, 12A104 (2020).

[51] R. Shindou, R. Matsumoto, S. Murakami, and J.-I. Ohe, Topological chiral magnonic edge mode in a magnonic crystal, Phys. Rev. B **87**, 174427 (2013).

[52] B. Ma and G. A. Fiete, Antiferromagnetic insulators with tunable magnon-polaron Chern numbers induced by in-plane optical phonons, Phys. Rev. B **105**, L100402 (2022).

[53] M. V. Berry, The quantum phase, five years after, in *Geometric Phases in Physics*, edited by A. Shapere and F. Wilczek (World Scientific, Singapore, 1989), pp. 7–28.

[54] K. Hwang, N. Trivedi, and M. Randeria, Topological magnons with nodal-line and triple-point degeneracies: Implications for thermal Hall effect in pyrochlore iridates, Phys. Rev. Lett. **125**, 047203 (2020).

[55] D. J. Thouless, M. Kohmoto, M. P. Nightingale, and M. den Nijs, Quantized Hall conductance in a two-dimensional periodic potential, Phys. Rev. Lett. **49**, 405 (1982).

[56] K. Nakata and G. Tatara, Magnon pumping by a time-dependent transverse magnetic field in ferromagnetic insulators, J. Phys. Soc. Jpn. **80**, 054602 (2011).

[57] J. Shi, P. Zhang, D. Xiao, and Q. Niu, Proper definition of spin current in spin-orbit coupled systems, Phys. Rev. Lett. **96**, 076604 (2006).

[58] A. Mook, R. R. Neumann, J. Henk, and I. Mertig, Spin Seebeck and spin Nernst effects of magnons in noncollinear antiferromagnetic insulators, Phys. Rev. B **100**, 100401(R) (2019).

[59] S. M. Rezende, Fundamentals of magnonics, in *Lecture Notes in Physics*, Vol. 969 (Springer, Cham, Switzerland, 2020).

[60] G. Wellein, H. Fehske, and A. P. Kampf, Peierls dimerization with nonadiabatic spin-phonon coupling, Phys. Rev. Lett. **81**, 3956 (1998).

[61] C. K. Majumdar and D. K. Ghosh, On next-nearest-neighbor interaction in a linear chain, J. Math. Phys. **10**, 1388 (1969).

[62] W. Shiramura, K.-I. Takatsu, H. Tanaka, K. Kamishima, M. Takahashi, H. Mitamura, and T. Goto, High-field magnetization processes of double spin chain systems $KCuCl_3$ and $TlCuCl_3$, J. Phys. Soc. Jpn. **66**, 1900 (1997).

[63] S. Bettler, L. Stoppel, Z. Yan, S. Gvasaliya, and A. Zheludev, Sign switching of dimer correlations in $SrCu_2(BO_3)_2$ under hydrostatic pressure, Phys. Rev. Res. **2**, 012010(R) (2020).

[64] O. V. Pylypovskyi, S. F. Weber, P. Makushko, I. Veremchuk, N. A. Spaldin, and D. Makarov, Surface-symmetry-driven Dzyaloshinskii–Moriya interaction and canted ferrimagnetism in collinear magnetoelectric antiferromagnet Cr_2O_3, arXiv:2310.13438.

[65] V. Arjona and M. A. H. Vozmediano, Rotational strain in Weyl semimetals: A continuum approach, Phys. Rev. B **97**, 201404(R) (2018).